GEOPHYSICS, VOL. 85, NO. 1 (JANUARY-FEBRUARY 2020); P. KS29–KS38, 11 FIGS.
10.1190/GEO2018-0861.1





# An adapted eigenvalue-based filter for ocean ambient noise processing

Guoli Wu[1], Hefeng Dong[2], Ganpan Ke[3], and Junqiang Song[4]

## ABSTRACT

Accurate approximations of Green's functions retrieved from the correlations of ambient noise require a homogeneous distribution of random and uncorrelated noise sources. In the real world, the existence of highly coherent, strong directional noise generated by ships, earthquakes, and other human activities can result in biases in the ambient-noise crosscorrelations (NCCs). We have developed an adapted eigenvalue-based filter to attenuate the interference of strong directional sources. The filter is based on the statistical model of the sample covariance matrix and can separate different components of the data covariance matrix in the eigenvalue spectrum. To improve the effectiveness and make it adaptable for different data sets, a weight is introduced to the filter. Then, the NCCs can be calculated directly from the filtered data covariance matrix. This approach is applied to a 1.02 h data set of ambient noise recorded by a permanent reservoir monitoring receiver array installed on the seabed. The power spectral density indicates that the noise recordings were contaminated by strong directional noise over nearly half of the whole observation period. Beamforming and crosscorrelation results indicate that the interference still exists even after applying traditional temporal and spectral normalization techniques, whereas the adapted eigenvalue-based filter can significantly attenuate it and help to obtain improved crosscorrelations. The approach makes it possible to retrieve reliable approximations of Green's functions over a much shorter recording time.

## INTRODUCTION

Over the past few decades, the reconstruction of Green's functions from the crosscorrelations of diffuse noise fields (CDNFs) has become a popular technique in ambient-noise tomography. The main idea of this technique is the extraction of expected waves (predominantly surface waves) from ambient-noise recordings without any active sources and knowledge of the environment. This idea initially originated from Aki (1957) and was further developed in the early 2000s. Rickett and Claerbout (1999) state that the crosscorrelation function of the noise recorded by two passive sensors equals the direct pulse response received when one of the sensors is treated as a source in helioseismology. Weaver and Lobkis (2001a, 2001b) find similar equivalence in diffuse acoustic fields and demonstrate it by a theoretical derivation in finite systems and laboratory ultrasonic experiments. Roux and Fink (2003) explore the reconstruction of Green's functions in underwater acoustics. Later, they investigate the recovery of coherent wavefronts using ocean ambient noise (Roux et al., 2004). Derode et al. (2003) extend this theory and confirm the possibility to recover Green's functions in infinite open systems as well. Campillo and Paul (2003) apply this technique to seismology using diffuse seismic coda and show the possibility to retrieve surface waves using the diffuse noise generated by distant sources. Shapiro and Campillo (2004) extract coherent Rayleigh waves from ambient seismic waves and compute the period group-velocity diagram that showed good consistency with previously predicted Rayleigh-wave tomographic maps. Later, they carry out surface-wave tomography using the extracted Rayleigh-wave Green's functions from long seismic noise sequences (Shapiro et al., 2005).

The success of these early attempts has made this technique an expanding research hot topic. Nowadays, surface-wave tomography

Manuscript received by the Editor 14 December 2018; revised manuscript received 25 September 2019; published ahead of production 21 October 2019; published online 6 December 2019.
[1]National University of Defense Technology, College of Meteorology and Oceanology, 410073 Changsha, China, National University of Defense Technology, College of Computer, 410073 Changsha, China, and Norwegian University of Science and Technology, Department of Electronic Systems, 7491 Trondheim, Norway. E-mail: wuguoli13@nudt.edu.cn.
[2]Norwegian University of Science and Technology, Department of Electronic Systems, 7491 Trondheim, Norway. E-mail: hefeng.dong@ntnu.no.
[3]Equinor ASA, Arkitekt Ebbells Vei 10, 7005 Trondheim, Norway. E-mail: gank@equinor.com.
[4]National University of Defense Technology, College of Meteorology and Oceanology, 410073 Changsha, China. E-mail: junqiang@nudt.edu.cn.

based on CDNF has been done at different scales ranging from hundreds of meters to thousands of kilometers (Chávez-García and Luzón, 2005; Gouédard et al., 2008; De Nisco and Nunziata, 2011; Li et al., 2012; Zhang and Gerstoft, 2014; Haned et al., 2015). Besides, it has been proven that body waves can be reconstructed from ambient noise (Roux et al., 2005a; Schimmel et al., 2011; Nakata et al., 2014; Olivier et al., 2015), although it is much more difficult than surface waves (Forghani and Snieder, 2010). Moreover, considering temporal subsurface changes, CDNFs are also applied to the passive monitoring area (e.g., Mordret et al., 2014; Brenguier et al., 2015; Wu et al., 2016; Delaney et al., 2017).

Accurate approximation of Green's functions between receiver pairs relies on several strict requirements of the CDNF (Draganov et al., 2003, 2006, 2010; Wapenaar and Fokkema, 2006; Mikesell et al., 2009; Fichtner et al., 2016; Delaney et al., 2017). One of the main requirements is that the noise field should be diffuse and equipartitioned (Weaver, 2010), which means that all modes must have equal amplitude and must be uncorrelated. To get a perfect equipartitioned diffuse wavefield, the noise should be generated by homogeneously distributed, uncorrelated sources (Derode et al., 2003; Wapenaar, 2004; Weaver and Lobkis, 2006). However, this requirement is difficult to meet in the real world. Noise sources usually tend to be nonstationary and heterogeneously distributed (Shapiro et al., 2006; Seydoux et al., 2016; Delaney et al., 2017), resulting in traveltime biases, spurious arrivals, and asymmetry features in the retrieved Green's functions (Tsai, 2009, 2011; Froment et al., 2010; Fichtner, 2014; Fichtner et al., 2016).

To overcome these drawbacks introduced by the directional nature of ambient noise and obtain a good estimation of the Green's function, performing the CDNF over long observation periods has been chosen as a solution by some researchers. The observation periods needed normally span from days (De Ridder and Biondi, 2013) to months (Shapiro et al., 2005; Bensen et al., 2007; Haned et al., 2015; Behm et al., 2016). In addition, numerous preprocessing techniques have been proposed to improve the emergence of the Green's function in the past few decades. Most of these techniques can be generally divided into two categories: individual approaches and array-based approaches. The individual approaches work on individual raw data recorded by one receiver. Most classical techniques belong to this category, such as 1-bit normalization (Campillo and Paul, 2003; Larose et al., 2004; Hanasoge and Branicki, 2013), the data-clipping approach using an appropriate chosen amplitude threshold (Sabra et al., 2005b), the data selection approach (Pedersen and Krüger, 2007; Groos and Ritter, 2009; Groos et al., 2012), and temporal and spectral domain normalization approaches (Bensen et al., 2007). Many array-based approaches have also been proposed to reduce the influence of strong directional sources and enhance the quality of retrieved Green's function in recent years. Instead of individual raw data, array data are usually used in these approaches, such as the passive inverse filter approach, which is based on the constructed noise-filtered matrix and working directly on the crosscorrelations (Gallot et al., 2012), the spatiotemporal filter approach, which is based on a beamforming formulation and working on the sample covariance matrix (SCM) (Leroy et al., 2012), and the spatial filter approach, which can filter the array data and cut down contributions of sources at a given direction (Carriere et al., 2014). Moreover, in ocean acoustics, Menon et al. (2012c) propose a novel method to isolate the diffuse component of the ocean noise field. The random matrix theory (RMT) (Menon et al., 2012a) is used to model the behavior of the eigenvalues of the noise SCM. Then, sequential hypothesis tests are applied to the SCM eigenvalues, rejecting strong, directional noise components based on the statistical model. Seydoux et al. (2017) develop a spatial equalization approach to attenuate the influence of strong directive seismic sources. An eigenvalue cutoff is derived theoretically, and the eigenvalues of the SCM are normalized based on it.

This work attempts to perform the CDNF over much shorter time periods, using ambient noise recorded by ocean-bottom cables. In this study, an adapted eigenvalue-based filtering technique is proposed by introducing a weight to the eigenvalue-based preprocessing method (Menon et al., 2012c; Seydoux et al., 2017) to improve the effectiveness of this method, considering the existence of local incoherent noise. The contribution of this paper lies in generalizing the strategies previously presented by Menon et al. (2012c) and Seydoux et al. (2017), and making it possible to extract reliable surface-wave dispersion measurements over much shorter recording time.

The paper is organized as follows: First, we summarize some preliminaries and definitions of the Green's function retrieval approach. The adapted eigenvalue-based filtering technique is introduced based on the statistical model of the SCM. Then, we describe the noise-recording array and the data processing procedure. We also investigate the temporal and spectral property of the noise used in this study. Later, the data analysis and results, including beamforming analysis, Green's function retrieval, and dispersion curve extraction, are presented to extensively evaluate the effectiveness of the proposed approach. Finally, we summarize the work and draw some conclusions.

## METHODOLOGY

### Green's function retrieval

Analytic derivations show that the time derivative of the noise crosscorrelation (NCC) $C_{ij}$ between two sensors $i$ and $j$ (located at $\mathbf{r}_i$ and $\mathbf{r}_j$, respectively) is approximately proportional to the time-domain Green's function (Snieder, 2004; Roux et al., 2005b; Sabra et al., 2005a):

$$\frac{dC_{ij}(t)}{dt} \sim -G(\mathbf{r}_i;\mathbf{r}_j,t) + G(\mathbf{r}_i;\mathbf{r}_j,-t), \tag{1}$$

where $C_{ij}(t)$ is the NCC function and $G(\mathbf{r}_i;\mathbf{r}_j,t)$ denotes the Green's function between source $i$ and receiver $j$. This relationship holds when the noise field is diffuse.

The NCC function $C_{ij}(t)$ is defined as the integration of two ambient-noise records $s_i(t)$ and $s_j(t)$

$$C_{ij}(t) = \int_0^T s_i(\tau)s_j(\tau+t)d\tau, \tag{2}$$

where $T$ denotes the observation period. In practice, the time-domain NCC function of the data $\hat{C}_{ij}(t)$ is often computed with

$$\hat{C}_{ij}(t) = \mathcal{F}^{-1}[\hat{R}_{ij}(f)], \tag{3}$$

where $\mathcal{F}^{-1}$ represents the inverse Fourier transform and $\hat{R}_{ij}(f)$ is the entry of the SCM at frequency $f$.

## Estimation of the SCM

With real noise data recorded by an $N$-sensor array, the SCM $\hat{\mathbf{R}}(f)$ is estimated in the frequency domain as

$$\hat{\mathbf{R}}(f) = \frac{1}{M}\sum_{m=1}^{M}\mathbf{u}_m(f)\mathbf{u}_m(f)^H, \tag{4}$$

where $\mathbf{u}_m(f)$ is the $N$-element Fourier coefficients vector of the $m$th time segment of the data at a particular frequency $f$, $H$ denotes the Hermitian transpose, and $M$ is the number of segments. In fact, it is sufficient to obtain a good estimation $\mathbf{R}(f)$ if $M$ is three times larger than $N$ (Menon et al., 2012a).

## Statistical model of the SCM

Following Gerstoft et al. (2012), we assume a data model $\mathbf{u}$ as

$$\mathbf{u} = \mathbf{s} + \mathbf{n}_c + \mathbf{n}_i, \tag{5}$$

where $\mathbf{s} = \sum_{k=1}^{K} S_k\mathbf{s}_k$ represents $K$ ($\ll N$) independent sources with direction $\mathbf{s}_k$ and complex amplitude $S_k$, $\mathbf{n}_c \sim \mathcal{CN}(\mathbf{0}, \sigma_c^2\mathbf{R}_c)$ represents the incoherent propagating seismic noise, and $\mathbf{n}_i \sim \mathcal{CN}(\mathbf{0}, \sigma_i^2\mathbf{I})$ represents incoherent noise (e.g., electronic noise and sensor self-noise), which is nonpropagating and uncorrelated between the sensors.

Assuming $\mathbf{s}$, $\mathbf{n}_c$, and $\mathbf{n}_i$ are uncorrelated with each other, the covariance matrix is computed as

$$\begin{aligned}\mathbf{R} = E(\mathbf{u}\mathbf{u}^H) &= \sum_{k=1}^{K}|S_k|^2\mathbf{s}_k\mathbf{s}_k^H + \sigma_c^2\mathbf{R}_c + \sigma_i^2\mathbf{I}\\ &= \mathbf{R}_s + \sigma_c^2\mathbf{R}_c + \sigma_i^2\mathbf{I},\end{aligned} \tag{6}$$

where $E$ denotes the expected value and $\mathbf{I}$ is an $N \times N$ identity matrix.

If a 2D noise field is considered (which is the case for surface waves), the propagating noise covariance matrix is proportional to the analytical covariance matrix of 2D isotropic noise field derived by Cox (1973):

$$[\mathbf{R}_c]_{ij} = J_0(2\pi f\gamma\|\mathbf{r}_i - \mathbf{r}_j\|), \tag{7}$$

where $f$ denotes the frequency, $J_0$ denotes the zeroth-order Bessel function of the first kind, $\gamma$ denotes the considered wave slowness, and $\mathbf{r}_i$ denotes the position of the receiver $i$, leading $\|\mathbf{r}_i - \mathbf{r}_j\|$ to be the distance between the receivers $i$ and $j$. If a 3D field is considered, one can find another alternative formula to replace equation 7 in Cox (1973).

The statistical model of the SCM $\hat{\mathbf{R}}_c$ relating to a diffuse noise field can be defined as (Mestre, 2008; Menon et al., 2012b, 2012c)

$$\hat{\mathbf{R}}_c = \frac{1}{M}\mathbf{R}_c\mathbf{X}\mathbf{X}^H, \tag{8}$$

where $\mathbf{X}$ is an $N \times M$ random matrix with entries $\mathbf{X}_{ij} \sim \mathcal{CN}(0, 1)$. If $L$ Monte Carlo trials are applied to equation 8, the empirical cumulative distribution of the largest eigenvalue of $\hat{\mathbf{R}}_c$ can be defined as

$$\mathrm{P}_{\max|\hat{\mathbf{R}}_c}(x) = \frac{\{a_n \le x\}}{L}, \tag{9}$$

where $a_1, \ldots, a_L$ are the largest eigenvalues of $\hat{\mathbf{R}}_c$ from each trial, denotes the cardinality of the set, and $\max|\hat{\mathbf{R}}_c$ denotes the largest eigenvalue of $\hat{\mathbf{R}}_c$.

## Adapted eigenvalue-based filtering technique

The definition of SCM makes it a positive semidefinite Hermitian matrix that only has nonnegative eigenvalues. Similar to Menon et al. (2012c), the objective of this approach is to isolate different components of $\hat{\mathbf{R}}$ based on the eigenvalue behavior of the statistical model as

$$\begin{aligned}\hat{\mathbf{R}} &= \sum_{k=1}^{K}\hat{\lambda}_k\hat{\mathbf{v}}_k\hat{\mathbf{v}}_k^H + \sum_{k=K+1}^{N'}\hat{\lambda}_k\hat{\mathbf{v}}_k\hat{\mathbf{v}}_k^H + \sum_{k=N'+1}^{N}\hat{\lambda}_k\hat{\mathbf{v}}_k\hat{\mathbf{v}}_k^H\\ &= \hat{\mathbf{R}}_s + \hat{\mathbf{R}}_d + \hat{\mathbf{R}}_i,\end{aligned} \tag{10}$$

where $\hat{\lambda}_1 > \hat{\lambda}_2 > \ldots > \hat{\lambda}_N \ge 0$ are the eigenvalues of $\hat{\mathbf{R}}$, $\hat{\mathbf{R}}_s$ is the strong, directional noise-related component, $\hat{\mathbf{R}}_d$ is the diffuse noise-related component, and $\hat{\mathbf{R}}_i$ is the uncorrelated noise-related component.

Note that it is difficult to match each strong source to a particular eigenvalue because some sources might have multiple effects over several eigenvalues (Baggeroer and Cox, 1999). Melo et al. (2010, 2013) also do a related analysis. They study the singular-value spectrum of the crosscorrelogram (the crosscorrelations in a time-space format) using singular-value decomposition. Their analogy indicates that the sources in the stationary region may spread over different singular vectors, and mostly contributes to the largest singular values. The field data example (Melo et al., 2013) indicates the difficulty in relating certain events to certain singular values.

Moreover, $\hat{\mathbf{R}}_s$ also contains a diffuse noise-related component and an uncorrelated noise-related component and $\hat{\mathbf{R}}_d$ also contains an uncorrelated noise-related component, which means a precise separation of $\hat{\mathbf{R}}$ into the three components in equation 6 is not possible.

The separation of $\hat{\mathbf{R}}$ turns out to be the determination of values for $K$ and $N'$. At any given frequency, once $K$ and $N'$ are determined, the strong, directional noise-related component and the uncorrelated noise-related component can be filtered, keeping only the diffuse noise-related component in the SCM $\hat{\mathbf{R}}$. In this approach, the eigenvalues of $\hat{\mathbf{R}}_s$ are reweighted to the largest eigenvalue of $\hat{\mathbf{R}}_d$ as

$$\hat{\lambda}_i = \hat{\lambda}_{K+1}, i = 1, \ldots, K, \tag{11}$$

and the eigenvalues of $\hat{\mathbf{R}}_i$ are filtered as

$$\hat{\lambda}_i = 0, i = N' + 1, \ldots, N. \tag{12}$$

### *The determination of number $N'$*

Because all eigenvalues above the cutoff number $N'$ are set to 0, an appropriate chosen cutoff value is important to make sure that the seismic wavefield can be fully described with $N'$ eigenvalues and the influence of uncorrelated noise can be well depressed. The eigenvalue cutoff number $N'$ used here was theoretically derived

by Seydoux et al. (2017) depending on the geometry and the degrees of freedom of considered wavefield. For a 2D wavefield case, the cutoff value is defined as

$$N'(f) = \min\{2[2\pi f\gamma\bar{r}] + 1, N/2\}, \tag{13}$$

where $[x]$ is the least integer greater than or equal to $x$, $\gamma$ is the slowness of the medium, and $\bar{r}$ is the typical separation of the array that represents the average interreceiver distance. The term $\bar{r}$ is defined as

$$\bar{r} = \frac{2}{N(N-1)}\sum_{i=1}^{N}\sum_{j>i}^{N} r_{ij}, \tag{14}$$

where $r_{ij}$ is the great-circle distance between two sensors $i$ and $j$.

*The determination of number K*

Following Johnstone (2001) and Menon et al. (2012c), a statistical inference method is used to determine $K$. We attempt to identify strong, directional noise-related eigenvalues of $\hat{\mathbf{R}}$ with a statistical hypothesis test.

At each frequency $f$, the eigenvalues $\{\hat{\lambda}_1, \ldots, \hat{\lambda}_{N'-1}\}$ of $\hat{\mathbf{R}}$ are tested sequentially at each step $k$ against the null and alternative hypotheses:

$$\begin{aligned}\mathcal{H}_0&: \texttt{This eigenvalue belongs to } \hat{\mathbf{R}}_d\\ \mathcal{H}_1&: \texttt{This eigenvalue belongs to } \hat{\mathbf{R}}_s.\end{aligned} \tag{15}$$

Starting with $k = 1$, the test continues until $\mathcal{H}_0$ no longer can be rejected, which means that the remaining $N' - k$ eigenvalues are not associated with the strong directional source(s).

The test statistic,

$$\tau(k) = \frac{\hat{\lambda}_k}{\bar{\sigma}_k}, \tag{16}$$

is used at step $k$, with

$$\bar{\sigma}_k = \frac{\sum_{i=k}^{N'}\hat{\lambda}_i}{N' - k + 1}, \tag{17}$$

where $\bar{\sigma}(k)$ is a normalization factor that makes $\tau(k)$ comparable to the analytical results at the same average power. The term $N'$ is used in this approach instead of $N$ because it is shown empirically that including eigenvalues of $\hat{\mathbf{R}}_i$ (which are very small compared with other eigenvalues) makes the test statistic too large, leading to an abnormal high-rejection probability of $\mathcal{H}_0$ (Menon et al., 2012c).

The null hypothesis $\mathcal{H}_0$ in equation 15 is rejected at a significance level $\alpha$ if

$$\tau(k) > w\mathrm{P}^{-1}_{\max|\hat{\mathbf{R}}_c^{N-k+1}}(1-\alpha), \tag{18}$$

where $\mathrm{P}_{\max|\hat{\mathbf{R}}_c^{N-k+1}}$ is the empirical cumulative distribution of the largest eigenvalue of an $N - k + 1$ dimensional SCM $\hat{\mathbf{R}}_c^{N-k+1}$, which can be precomputed by 1000 Monte Carlo trials. The significance level $\alpha = 0.05$ is used in this paper. We introduce a weight $w$ $(0 \le w \le 1)$ to this hypothesis test here because the existence of incoherent noise components in $\hat{\mathbf{R}}_c^{N-k+1}$ will reduce the value of $\tau(k)$. In addition, the threshold determined by the hypothesis test approach might not be equal to the exact threshold for strong, directional noise in the real world. An appropriately selected $w$ can compensate these drawbacks and improve the effectiveness of this approach.

The introduction of the weight here actually generalizes the two approaches proposed by Menon et al. (2012c) and Seydoux et al. (2017). When $w = 0$, all eigenvalues tested are rejected and reweighted to the same value according to equation 11. Then, this approach actually converges to the spatial equalization method proposed by Seydoux et al. (2017). When $0 < w < 1$, this approach can be recognized as a relaxed version of the spatial equalization method, which can keep more original information of the diffused noise component and show an improved performance compared with $w = 1$. When $w = 1$, this approach is working in the same way with Menon et al. (2012c), except the slight difference on the determination of $N'$.

## NOISE RECORDING AND PROCESSING

The ocean wave-related noise data studied in this paper were recorded by a straight cable of a permanent reservoir monitoring (PRM) receiver array. The cable contains 254 hydrophones with a spacing of 50 m for a total cable length of 12.65 km. In addition to normal active seismic sources, passive seismic data were acquired during those periods outside active PRM operations. The data used here were continuously recorded for 1.02 h at a sampling rate of 500 Hz on 14 September 2015.

The raw noise recording for one receiver and its spectrogram are shown in Figure 1. As is shown in Figure 1a, the noise recording is contaminated by unknown events with large amplitudes, high energy, and directional property (which is shown in a beamforming study later). Although most of the energy of the unknown events spreads in the frequencies larger than 4 Hz (Figure 1b), the NCCs might be affected significantly.

The power spectral density is presented in Figure 2. It shows a clear peak at 0.09 Hz, which can most likely be recognized as infragravity waves generated mostly by surf breaking at coastlines (Olofsson, 2010). The microseisms, spanning from 0.2 to 4.5 Hz, are believed to be generated by nonlinear wave-wave interaction of wind-generated ocean gravity waves traveling in opposite directions (Olofsson, 2010). Therefore, the microseisms are thought to be more evenly distributed in the ocean and the Green's functions are retrieved over the frequency band 0.2–4.5 Hz in this study. Strong directional sources, including earthquakes, ship noise, and other sources with high energy, dominate the spectrum beyond 4.5 Hz.

To retrieve the empirical Green's function from the ambient noise, several preprocessing steps are applied to the data recorded by each sensor individually. First, the data are demeaned, detrended (Bensen et al., 2007), and band-pass filtered between 0.2 and 4.5 Hz. Then, 1-bit normalization is applied to the filtered data to reduce the effect of energetic arrivals in the time domain. This step is done by keeping only the sign of the signal. Then, the normalized data are divided into nine blocks with 405 s each, and each block is further segmented into $M = 90$ segments of 4.5 s. After that, Fourier transform is applied to each segment, and the SCM for each frequency $\hat{\mathbf{R}}(f)$ is computed using equation 4 for each block, with $N = 30$ and $M = 90$. Finally, the eigenvalues of the SCM are computed and filtered by the adapted eigenvalue filter, and the filtered

SCMs are stacked over blocks before calculating the NCC using equation 3.

## DATA ANALYSIS AND RESULTS

### Beamforming analysis

To evaluate the isotropic nature of the noise field, conventional beamforming is performed for each block at several frequencies. The beam power is estimated with respect to the incident angle as

$$B(f,\theta) = \mathbf{b}^H(f,\theta)\hat{\mathbf{R}}(f)\mathbf{b}(f,\theta), \qquad (19)$$

where $\theta$ is the incident angle, $\mathbf{b}(f,\theta)$ is the plane-wave beamformer, with the $n$th entry given by $b_n(f,\theta) = e^{-2i\pi f n d \sin(\theta)/\hat{v}}$, in which $\hat{v}$ is the phase speed of the surface wave and $d$ is the interstation spacing. We estimate the phase speed based on the profile of Snorre field (a reservoir that is very close to the Grane field studied here; Li et al., 2012). An estimated phase speed $\hat{v} = 1000$ m/s is used in this study. Although the dispersion feature of the surface waves is ignored here, it does not make a big difference for this data set. Moreover, more accurate beamforming can be applied after the dispersion curves of the surface wave are extracted.

The beam power of the unfiltered SCM $\hat{\mathbf{R}}(f)$ is presented in Figure 3. It shows that the noise field is approximately isotropic over the entire duration at 1 Hz (Figure 3a), except for 30–35 min, when an unknown event with high energy happened at approximately −10°–20°. This event can be recognized more clearly at 2 and 3 Hz in Figure 3b and 3c, respectively. In addition, Figure 3a–3c indicates that noise signals coming from −20° to 20° turn stronger as the frequency increases. A source dominates the beam power at 4 Hz in Figure 3d, with an almost constant direction of 35°, which is recognized as the source of the unknown energetic events shown in Figure 1 considering the high consistency in time.

After applying the adapted eigenvalue-based filter, the filtered SCM $\hat{\mathbf{R}}'(f)$ is expected to be a good approximation to $\hat{\mathbf{R}}_d(\mathrm{f})$. Beamforming on the filtered SCM $\hat{\mathbf{R}}'(f)$ is presented in Figure 4b–4d and Figure 4f–4h at 2 and 4 Hz, respectively, for different weight values. When $w = 1$, only part of the strong directional power (caused by the unknown energetic events) can be removed (Figure 4b and 4f). The strong directional power drops relatively as the weight decreases. When the weight decreases to 0.2, most of the effect of the strong directional power is eliminated (Figure 4c and 4g). When the weight decreases to 0, this approach is working exactly as the spatial equalization method proposed by Seydoux et al. (2017), and the beamforming results (Figure 4d and 4h) do not show big improvements compared to the case $w = 0.2$. Although the eigenvalue filter can remove most of the strong, directional power, the beam power between −45° and 45° is still a little higher compared with other directions (approximately 5 dB higher in

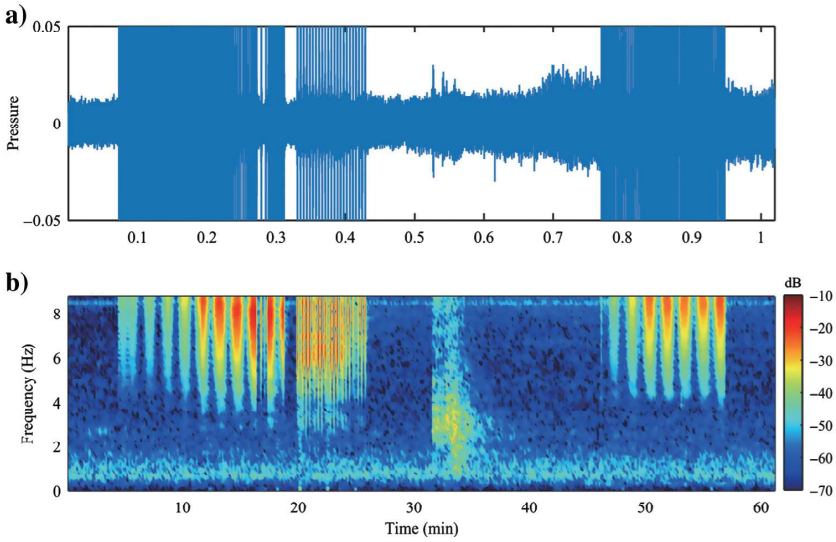


Figure 1. (a) The raw noise recording at one sensor. Because the amplitude of pressure is not used in the proposed method, the pressure is normalized with the maximum amplitude. (b) The power spectral density (dB to 1 $Pa^2$/Hz) as a function of time and frequency (known as a spectrogram).

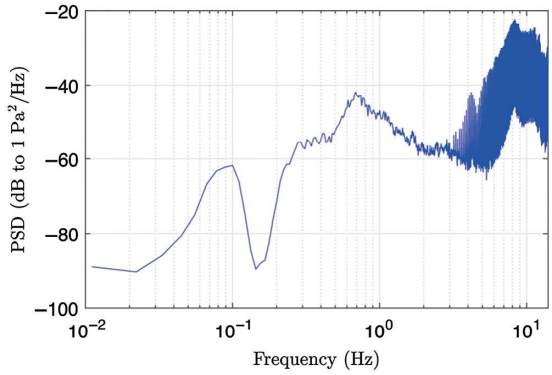


Figure 2. Power spectral density. Frequency axis is in logarithmic scale for display purposes.

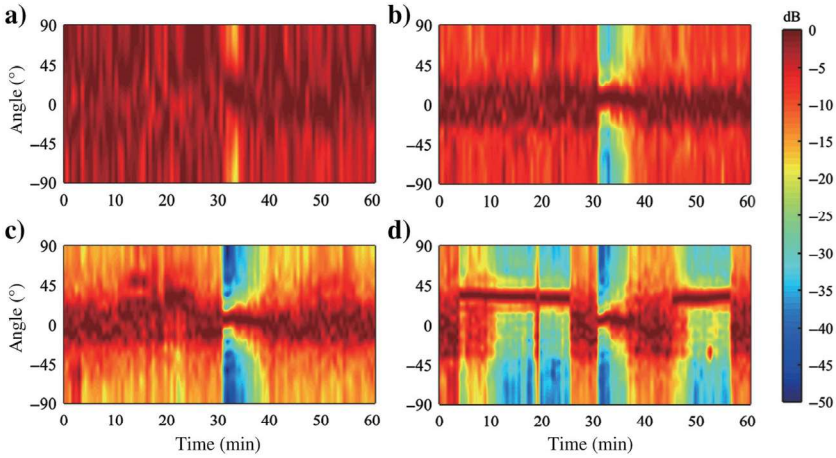


Figure 3. Conventional beamforming results (dB with the reference to the maximum energy) using the unfiltered SCM $\hat{\mathbf{R}}(f)$ at (a) 1 Hz, (b) 2 Hz, (c) 3 Hz, and (d) 4 Hz. The beam power is normalized at each time segment.

Figure 4h). A possible reason is that the sources between −45° and 45° are not strong enough and the effects of these sources are indistinguishable in the eigenvalue spectrum using this approach.

## Empirical Green's function retrieval

The raw NCC, rather than its time derivative, is often used as an approximation to the empirical Green's function (Derode et al., 2003; Roux et al., 2004; Gerstoft et al., 2008). The SCMs computed from consecutive blocks are stacked and averaged, and equation 3 is used to calculate the resulting NCC as $\langle \hat{C}_{ij}(t) \rangle_T = \mathcal{F}^{-1}[\langle \hat{\mathbf{R}}_{ij}(f) \rangle_T]$, where $T$ represents the averaging time. Thirty NCCs between 30 recording pairs are treated as one gather. The maximum distance for one gather is 1450 m. As is shown in Figure 5, we can have 225 gathers in this cable at most, with an overlap of 1400 m. Each gather contains the averaged information of the seabed structure covering 1450 m. In this study, we only focus on obtaining better NCCs for a single gather. A further lateral change of the seabed structure can be investigated, but it is beyond the scope of this paper.

The NCCs obtained using different approaches are presented in Figure 6. Note that all the NCCs are band-pass filtered between 0.2 and 4.5 Hz. The standard NCCs retrieved from the unfiltered SCM calculated using only classic temporal and spectral normalization (TSN) (Bensen et al., 2007) are shown in Figure 6a. The result is asymmetric, and the NCCs are apparently dominated by the unknown energetic events. As a result, the expected surface waves are shielded. Figure 6b and6c presents the NCCs retrieved from the filtered SCM $\hat{\mathbf{R}}'$. Most of the effect of the unknown energetic events is removed in Figure 6b, but some small peaks belonging to the unknown energetic events can still be recognized. The effect of the unknown energetic events turns invisible in Figure 6c, using the weight $w = 0.2$. Although the effect of the unknown energetic events is completely removed when the weight decreases to 0, spurious arrivals appear in Figure 6d. This phenomenon indicates that this approach turns too aggressive for these data when $w = 0$, normalizing all the eigenvalues of $\hat{\mathbf{R}}_s$ and $\hat{\mathbf{R}}_d$. It not only decreases the strong sources, but it also enhances some unexpected noise, causing spurious arrivals in the NCCs. These arrivals dominate the NCCs, and surface-wave arrivals are shielded.

To further enhance the signal-to-noise ratio of the NCCs, averaging of the positive and negative parts of NCC functions (Bensen et al., 2007; Fichtner et al., 2016) is used here. Averaging the positive and negative parts after the eigenvalue filtering can compensate these shortcomings and lead to more reasonable results. Figure 7 presents the comparison between the normal NCCs and averaged NCCs for $w = 0.2$. Figure 7b shows a clearer dispersion feature of the surface waves compared with Figure 7a. The case $w = 0.2$ in Figure 8 further shows the necessity of the averaging. Although the peaks at G and H in the case show good symmetry considering the time axis, they have different amplitudes due to the effect of the unknown energetic events.

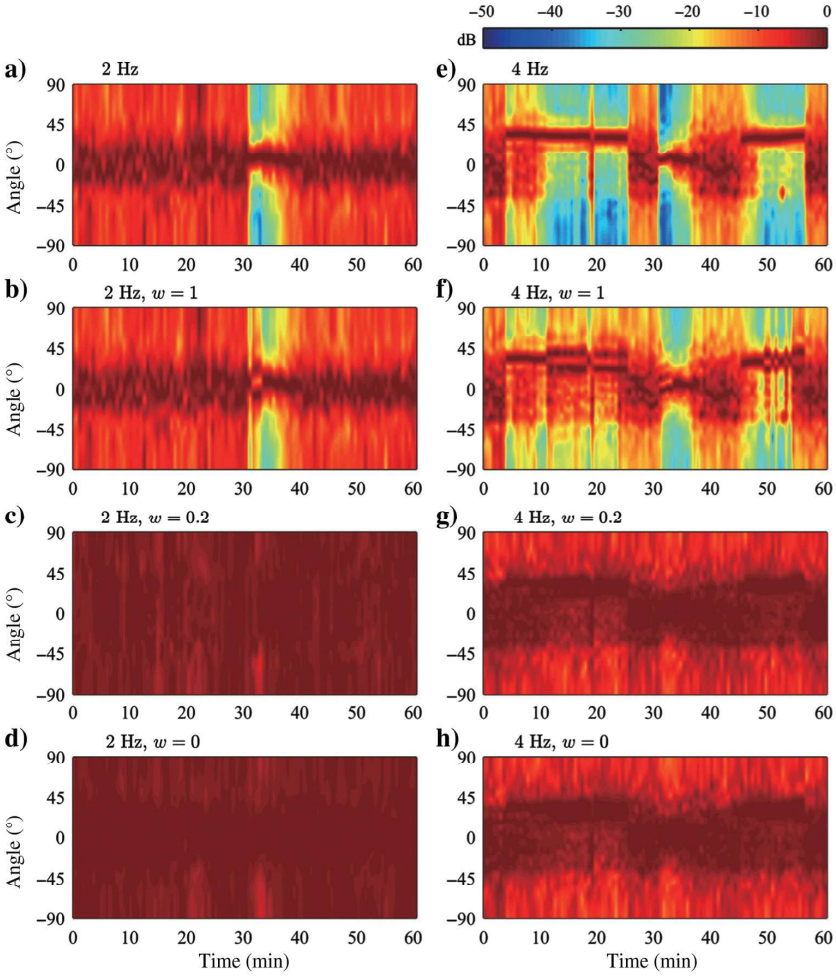


Figure 4. Conventional beamforming results (dB with reference to the maximum energy). (a and e) Results obtained using unfiltered SCM $\hat{\mathbf{R}}(f)$. (b-d and f-h) Results obtained using the filtered SCM $\hat{\mathbf{R}}'(f)$ with different values of weight. The beam power is normalized at each time segment.

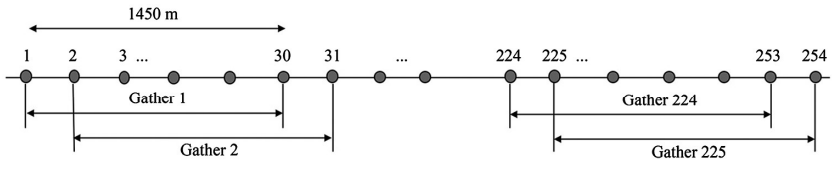


Figure 5. The cable geometry and gathers.

## Weight-selection study

The best weight for this approach should remove most of the effect of the strong sources and keep the useful information of the data as much as possible. Note that the best weight might be different for different data sets, which makes it a data-dependent parameter. Figure 8 presents the NCC functions retrieved with four representative weights at the distance 1250 m. The amplitudes of

these NCC functions are nominalized by the maximum of each line for display purposes. The dotted line denotes the NCC function retrieved from the SCM calculated using the TSN. Several peaks show up at the positive part of this NCC, which are recognized as the effect of the unknown energetic events. For the cases $w = 0.5$ (green line) and $w = 1$ (red line), the NCC functions are affected by these peaks belonging to the unknown energetic events at A, B, C, D, E, and F apparently, shown in Figure 8. As the weight decreases to 0.2, it shows an improved signal-to-noise ratio and better symmetry feature. Spurious arrivals appear when $w = 0$ (blue line), which means that some noise other than surface waves is enhanced unexpectedly, leading to biased traveltimes. More values of $w$ are studied, and it shows that a reasonable good result can be obtained using $w = 0.2$, which is selected for this data set.

The degree of symmetry of the NCCs is always considered as an indicator for more reasonable results. We define an asymmetry index $S$ to quantify the asymmetry as

$$S = \frac{\int_0^{T_0} |C(t) - C(-t)|^2 dt}{\int_{-T_0}^{T_0} |C(t)|^2 dt}, \qquad (20)$$

where $C(t)$ is the crosscorrelation function and $T_0$ is the time limit considered. In this way, smaller asymmetry index means better symmetry of the NCCs. We take $T_0 = 4.5$ s and plot the asymmetry index as a function of weight in Figure 9. It shows that the asymmetry index decreases steadily as the weight decreases from 1 to 0.2, indicating a better and better symmetry condition. But as the weight continues to decrease, the asymmetry index starts to increase, so decreasing the value of the weight cannot improve the quality of the crosscorrelations. Although better symmetry conditions can be reached for $w < 0.1$, spurious arrivals similar to Figure 6d start to arise and dominate the waveforms. Therefore, $w = 0.2$ is considered to be a good choice for this data set.

Note that if a long time recording is used, the weight should be considered as a time-dependent parameter as well because the number and coherence of the noise sources in this field might change over time. In this study, the weight is considered as a time-independent parameter because a very short-time recording is used.

## The extraction of dispersion curves

The slowness-frequency transform, a multisensor method, is used to extract the dispersion curves from the retrieved NCCs (McMechan and Yedlin, 1981). In this method, the signal amplitude is expressed as a function of frequency and phase speed in a Gabor diagram. An example of a Gabor diagram extracted from the ambient noise NCCs using eigenvalue filter with weight $w = 0.2$ is shown in Figure 10. Note that the amplitude is normalized independently at each frequency for display purposes. One fundamental and three

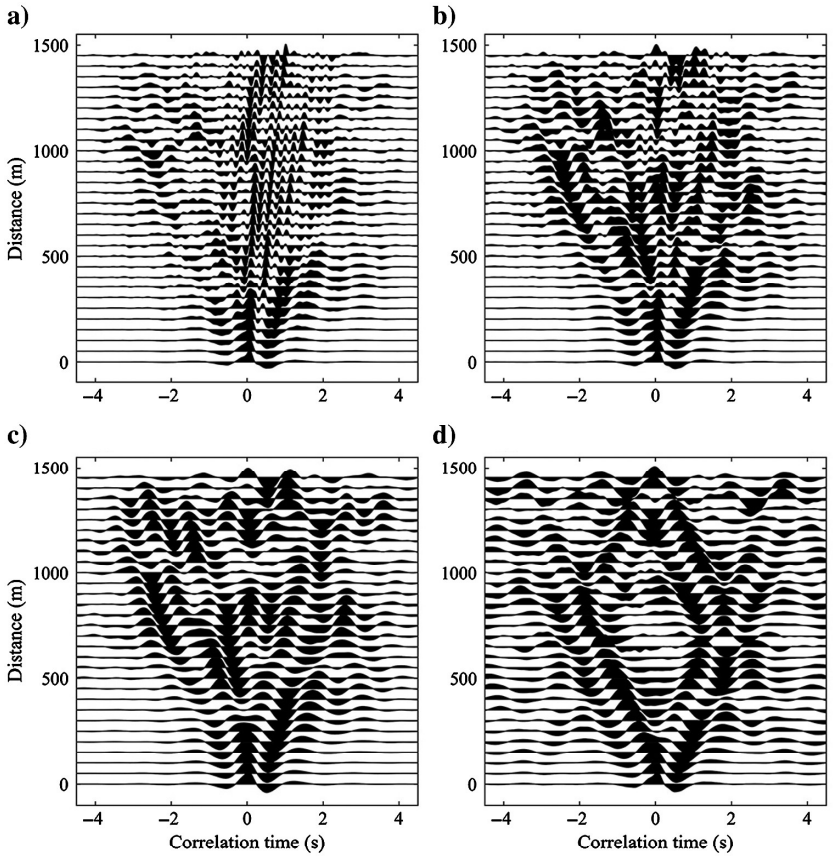


Figure 6. Comparison of the NCCs retrieved from the (a) unfiltered SCM calculated using the TSN and filtered SCM $\mathbf{R}'$ with different weights (b) $w = 1$, (c) $w = 0.2$, and (d) $w = 0$. The NCCs are band-pass filtered between 0.2 and 4.5 Hz.

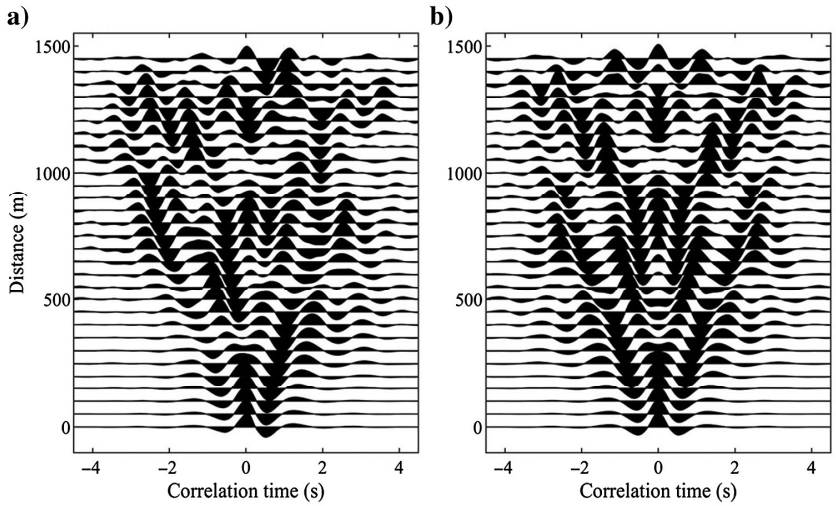


Figure 7. Comparison between (a) the normal NCCs and (b) averaged NCCs, with $w = 0.2$.

higher order modes can be recognized apparently over the investigated frequency band 0.2–4.5 Hz. The corresponding phase-speed dispersion curves are also extracted and indicated in Figure 10 with white dots.

An example of dispersion curves extracted using different approaches (or weights) is presented in Figure 11 for comparison. The fundamental modes of three approaches are well-matched in the frequency band 0.7–1.7 Hz. The fundamental mode and the second-order mode extracted using the TSN (black dots) are mixed together, due to the influence of strong, directional noise. Dispersion curves extracted using the adapted eigenvalue-based filter with $w = 1$ and $w = 0.2$ are roughly matched in all four modes. The influence of unknown energetic events in the case $w = 1$ (shown in Figures 4, 6, and 8) is thought to be the reason of the differences between $w = 1$ and $w = 0.2$. The differences can be either larger or smaller for different gathers in Figure 5. When $w = 0$, the curves (blue diamonds) become flat and do not show a good dispersion feature, which can be indicated by the waveforms in Figure 6d as well. That is because some unexpected noise is also enhanced under this condition and the expected surface waves are shielded.

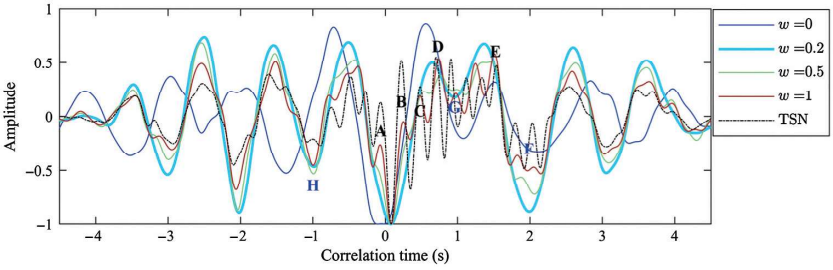


Figure 8. The NCC functions retrieved with different weights at a distance of 1250 m. The amplitudes are normalized by the maximum of each line for display purposes. The term $w$ denotes the weight and TSN denotes the classic temporal and spectral normalization method. The letters A–H mark different peaks for the NCC functions. The dotted line denotes the NCC functions using the unfiltered SCM.

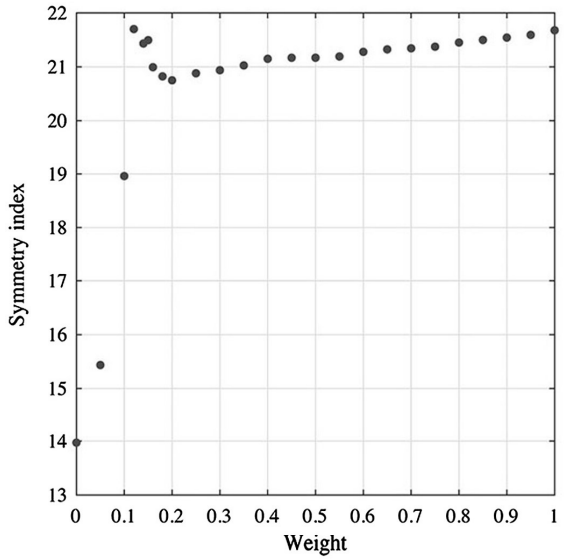


Figure 9. The asymmetry index as a function of weight.

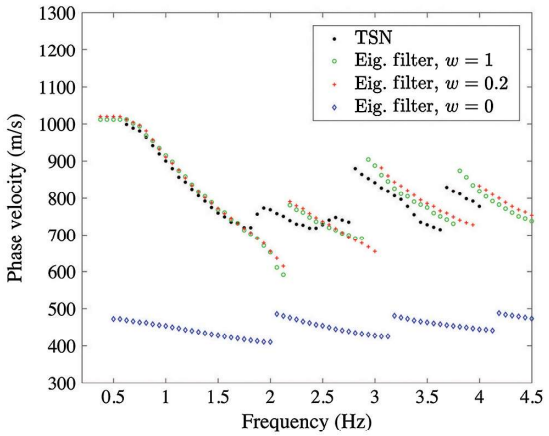


Figure 11. Comparison of different dispersion curves extracted using different approaches. The black dots, green circles, red plus signs, and blue diamonds denote dispersion curves extracted using the TSN, the adapted eigenvalue-based filtering technique with weight $w = 1$, $w = 0.2$, and $w = 0$, respectively.

Figure 10. Signal amplitude (dB) as a function of phase speed and frequency (normalized independently at each frequency for display purposes). The white dots denote the extracted dispersion curves from the Gabor diagram, in this case, $w = 0.2$.

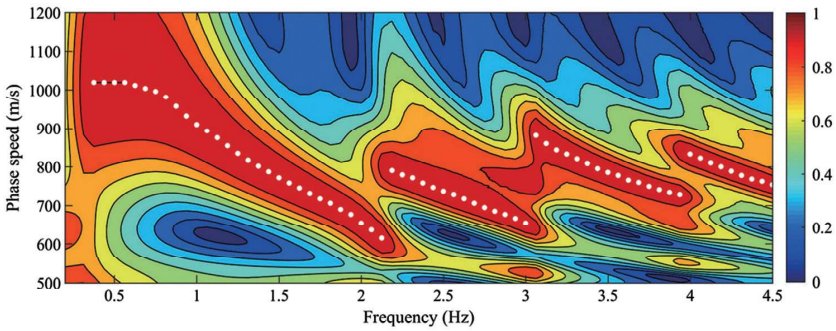

## CONCLUSION

We have proposed and applied an adapted eigenvalue-based filter to retrieve the surface wave part of Green's functions from ocean ambient noise recorded by a PRM array. Beamforming analysis shows that strong, directional noise still exists in the recordings, even after applying the traditional TSN techniques.

To get the wavefield closer to be equipartitioned, averaging the crosscorrelations over time and 1-bit normalization are used. Moreover, by separating different components in the eigenvalue spectrum of the SCM, the proposed eigenvalue-based filter significantly reduces the influence of stubborn, strong, directional sources and relatively reinforces the weak isotropic background noise. After using these methods mentioned earlier, the equipartitioned wavefield actually can be partially recovered, and a good-quality Green's function retrieval is ensured. The approach makes it possible to retrieve reliable surface-wave dispersion measurements over a much shorter recording time (approximately 1 h) even if the noise recordings are contaminated by strong directional noise over nearly half of the whole observation period.

An appropriate chosen filtering weight is important for this approach. The introduced weight generalizes previously proposed eigenvalue-based approaches and makes it adaptable for different data sets. Note that the weight is a data-dependent parameter, and it might be time-dependent if a long time recording is used. A careful weight-selection study must be implemented before this approach is applied, to attenuate the interference of strong directional noise sources and avoid spurious arrivals.

## ACKNOWLEDGMENTS

The authors would like to acknowledge Grane license partners (Equinor ASA, Petoro AS, ExxonMobil E&P Norway AS, and ConocoPhillips Skandinavia AS) for allowing to present this work. The views and opinions expressed in this paper are those of the authors and are not necessarily shared by the license partners.

This work is partially supported by the National Natural Science Foundation of China (grant no. 41605070). G. Wu also acknowledges the China Scholarship Council for the fellowship support (no. [2017]3109).

## DATA AND MATERIALS AVAILABILITY

Data associated with this research are confidential and cannot be released.

## REFERENCES

Aki, K., 1957, Space and time spectra of stationary stochastic waves, with special reference to microtremors: Bulletin of the Earthquake Research Institute, **35**, 415–456.

Baggeroer, A., and H. Cox, 1999, Passive sonar limits upon nulling multiple moving ships with large aperture arrays: Conference Record of the Thirty-Third Asilomar Conference on Signals, Systems, and Computers (Cat. No. CH37020), IEEE, 103–108.

Behm, M., N. Nakata, and G. Bokelmann, 2016, Regional ambient noise tomography in the eastern Alps of Europe: Pure and Applied Geophysics, **173**, 2813–2840, doi: 10.1007/s00024-016-1314-z.

Bensen, G., M. Ritzwoller, M. Barmin, A. Levshin, F. Lin, M. Moschetti, N. Shapiro, and Y. Yang, 2007, Processing seismic ambient noise data to obtain reliable broad-band surface wave dispersion measurements: Geophysical Journal International, **169**, 1239–1260, doi: 10.1111/j.1365-246X.2007.03374.x.

Brenguier, F., P. Kowalski, N. Ackerley, N. Nakata, P. Boué, M. Campillo, E. Larose, S. Rambaud, C. Pequegnat, T. Lecocq, P. Roux, V. Ferrazzini, N. Villeneuve, N. M. Shapiro, and J. Chaput, 2015, Toward 4D noise-based seismic probing of volcanoes: Perspectives from a large-n experiment on Piton de la Fournaise volcano: Seismological Research Letters, **87**, 15–25, doi: 10.1785/0220150173.

Campillo, M., and A. Paul, 2003, Long-range correlations in the diffuse seismic coda: Science, **299**, 547–549, doi: 10.1126/science.1078551.

Carriere, O., P. Gerstoft, and W. S. Hodgkiss, 2014, Spatial filtering in ambient noise interferometry: The Journal of the Acoustical Society of America, **135**, 1186–1196, doi: 10.1121/1.4863658.

Chávez-García, F. J., and F. Luzón, 2005, On the correlation of seismic microtremors: Journal of Geophysical Research: Solid Earth, **110**, B11313, doi: 10.1029/2005JB003671.

Cox, H., 1973, Spatial correlation in arbitrary noise fields with application to ambient sea noise: The Journal of the Acoustical Society of America, **54**, 1289–1301, doi: 10.1121/1.1914426.

De Nisco, G., and C. Nunziata, 2011, V S profiles from noise cross correlation at local and small scale: Pure and Applied Geophysics, **168**, 509–520, doi: 10.1007/s00024-010-0119-8.

De Ridder, S., and B. Biondi, 2013, Daily reservoir-scale subsurface monitoring using ambient seismic noise: Geophysical Research Letters, **40**, 2969–2974, doi: 10.1002/grl.50594.

Delaney, E., L. Ermert, K. Sager, A. Kritski, S. Bussat, and A. Fichtner, 2017, Passive seismic monitoring with nonstationary noise sources: Geophysics, **82**, no. 4, KS57–KS70, doi: 10.1190/geo2016-0330.1.

Derode, A., E. Larose, M. Tanter, J. De Rosny, A. Tourin, M. Campillo, and M. Fink, 2003, Recovering the Green's function from field-field correlations in an open scattering medium (l): The Journal of the Acoustical Society of America, **113**, 2973–2976, doi: 10.1121/1.1570436.

Draganov, D., R. Ghose, E. Ruigrok, J. Thorbecke, and K. Wapenaar, 2010, Seismic interferometry, intrinsic losses and q-estimation: Geophysical Prospecting, **58**, 361–373, doi: 10.1111/(ISSN)1365-2478.

Draganov, D., K. Wapenaar, and J. Thorbecke, 2003, Synthesis of the reflection response from the transmission response in the presence of white noise sources: 65th Annual International Conference and Exhibition, EAGE, Extended Abstracts, P218.

Draganov, D., K. Wapenaar, and J. Thorbecke, 2006, Seismic interferometry: Reconstructing the earth's reflection response: Geophysics, **71**, no. 4, SI61–SI70, doi: 10.1190/1.2209947.

Fichtner, A., 2014, Source and processing effects on noise correlations: Geophysical Journal International, **197**, 1527–1531, doi: 10.1093/gji/ggu093.

Fichtner, A., L. Stehly, L. Ermert, and C. Boehm, 2016, Generalised interferometry — 1: Theory for inter-station correlations: Geophysical Journal International, **208**, 603–638, doi: 10.1093/gji/ggw420.

Forghani, F., and R. Snieder, 2010, Underestimation of body waves and feasibility of surface-wave reconstruction by seismic interferometry: The Leading Edge, **29**, 790–794, doi: 10.1190/1.3462779.

Froment, B., M. Campillo, P. Roux, P. Gouedard, A. Verdel, and R. L. Weaver, 2010, Estimation of the effect of nonisotropically distributed energy on the apparent arrival time in correlations: Geophysics, **75**, no. 5, SA85–SA93, doi: 10.1190/1.3483102.

Gallot, T., S. Catheline, P. Roux, and M. Campillo, 2012, A passive inverse filter for Green's function retrieval: The Journal of the Acoustical Society of America, **131**, EL21–EL27, doi: 10.1121/1.3665397.

Gerstoft, P., W. S. Hodgkiss, M. Siderius, C.-F. Huang, and C. H. Harrison, 2008, Passive fathometer processing: The Journal of the Acoustical Society of America, **123**, 1297–1305, doi: 10.1121/1.2831930.

Gerstoft, P., R. Menon, W. S. Hodgkiss, and C. F. Mecklenbräuker, 2012, Eigenvalues of the sample covariance matrix for a towed array: The Journal of the Acoustical Society of America, **132**, 2388–2396, doi: 10.1121/1.4746024.

Gouédard, P., P. Roux, and M. Campillo, 2008, Small-scale seismic inversion using surface waves extracted from noise cross correlation: The Journal of the Acoustical Society of America, **123**, EL26–EL31, doi: 10.1121/1.2838251.

Groos, J., S. Bussat, and J. Ritter, 2012, Performance of different processing schemes in seismic noise cross-correlations: Geophysical Journal International, **188**, 498–512, doi: 10.1111/j.1365-246X.2011.05288.x.

Groos, J., and J. Ritter, 2009, Time domain classification and quantification of seismic noise in an urban environment: Geophysical Journal International, **179**, 1213–1231, doi: 10.1111/j.1365-246X.2009.04343.x.

Hanasoge, S. M., and M. Branicki, 2013, Interpreting cross-correlations of one-bit filtered seismic noise: Geophysical Journal International, **195**, 1811–1830, doi: 10.1093/gji/ggt337.

Haned, A., E. Stutzmann, M. Schimmel, S. Kiselev, A. Davaille, and A. Yelles-Chaouche, 2015, Global tomography using seismic hum: Geophysical Journal International, **204**, 1222–1236, doi: 10.1093/gji/ggv516.

Johnstone, I. M., 2001, On the distribution of the largest eigenvalue in principal components analysis: The Annals of Statistics, **29**, 295–327, doi: 10.1214/aos/1009210544.

Larose, E., A. Derode, M. Campillo, and M. Fink, 2004, Imaging from one-bit correlations of wideband diffuse wave fields: Journal of Applied Physics, **95**, 8393–8399, doi: 10.1063/1.1739529.

Leroy, C., S. Lani, K. G. Sabra, W. S. Hodgkiss, W. Kuperman, and P. Roux, 2012, Enhancing the emergence rate of coherent wavefronts from ocean ambient noise correlations using spatio-temporal filters: The Journal of the Acoustical Society of America, **132**, 883–893, doi: 10.1121/1.4731231.

Li, C., S. E. Dosso, H. Dong, D. Yu, and L. Liu, 2012, Bayesian inversion of multimode interface-wave dispersion from ambient noise: IEEE Journal of Oceanic Engineering, **37**, 407–416, doi: 10.1109/JOE.2012.2189922.

McMechan, G. A., and M. J. Yedlin, 1981, Analysis of dispersive waves by wave field transformation: Geophysics, **46**, 869–874, doi: 10.1190/1.1441225.

Melo, G., A. Malcolm, D. Mikessel, and K. Van Wijk, 2010, Using SVD for improved interferometric Green's function recovery: 80th Annual International Meeting, SEG, Expanded Abstracts, 3986–3990, doi: 10.1190/1.3513688.

Melo, G., A. Malcolm, D. Mikesell, and K. Van Wijk, 2013, Using SVD for improved interferometric Green's function retrieval: Geophysical Journal International, **194**, 1596–1612, doi: 10.1093/gji/ggt172.

Menon, R., P. Gerstoft, and W. S. Hodgkiss, 2012a, Asymptotic eigenvalue density of noise covariance matrices: IEEE Transactions on Signal Processing, **60**, 3415–3424, doi: 10.1109/TSP.2012.2193573.

Menon, R., P. Gerstoft, and W. S. Hodgkiss, 2012b, Asymptotic eigenvalue density of noise covariance matrices: IEEE Transactions on Signal Processing, **60**, 3415–3424, doi: 10.1109/TSP.2012.2193573.

Menon, R., P. Gerstoft, and W. S. Hodgkiss, 2012c, Cross-correlations of diffuse noise in an ocean environment using eigenvalue based statistical inference: The Journal of the Acoustical Society of America, **132**, 3213–3224, doi: 10.1121/1.4754558.

Mestre, X., 2008, On the asymptotic behavior of the sample estimates of eigenvalues and eigenvectors of covariance matrices: IEEE Transactions on Signal Processing, **56**, 5353–5368, doi: 10.1109/TSP.2008.929662.

Mikesell, D., K. van Wijk, A. Calvert, and M. Haney, 2009, The virtual refraction: Useful spurious energy in seismic interferometry: Geophysics, **74**, no. 3, A13–A17, doi: 10.1190/1.3095659.

Mordret, A., N. M. Shapiro, and S. Singh, 2014, Seismic noise-based time-lapse monitoring of the Valhall overburden: Geophysical Research Letters, **41**, 4945–4952, doi: 10.1002/2014GL060602.

Nakata, N., R. Snieder, and M. Behm, 2014, Body-wave interferometry using regional earthquakes with multidimensional deconvolution after wavefield decomposition at free surface: Geophysical Journal International, **199**, 1125–1137, doi: 10.1093/gji/ggu316.

Olivier, G., F. Brenguier, M. Campillo, R. Lynch, and P. Roux, 2015, Body-wave reconstruction from ambient seismic noise correlations in an underground mine: Geophysics, **80**, no. 3, KS11–KS25, doi: 10.1190/geo2014-0299.1.

Olofsson, B., 2010, Marine ambient seismic noise in the frequency range 1–10 Hz: The Leading Edge, **29**, 418–435, doi: 10.1190/1.3378306.

Pedersen, H. A., and F. Krüger, 2007, Influence of the seismic noise characteristics on noise correlations in the Baltic shield: Geophysical Journal International, **168**, 197–210, doi: 10.1111/j.1365-246X.2006.03177.x.

Rickett, J., and J. Claerbout, 1999, Acoustic daylight imaging via spectral factorization: Helioseismology and reservoir monitoring: The Leading Edge, **18**, 957–960, doi: 10.1190/1.1438420.

Roux, P., and M. Fink, 2003, Green's function estimation using secondary sources in a shallow water environment: The Journal of the Acoustical Society of America, **113**, 1406–1416, doi: 10.1121/1.1542645.

Roux, P., W. Kuperman, and N. Group, 2004, Extracting coherent wave fronts from acoustic ambient noise in the ocean: The Journal of the Acoustical Society of America, **116**, 1995–2003, doi: 10.1121/1.1797754.

Roux, P., K. G. Sabra, P. Gerstoft, W. Kuperman, and M. C. Fehler, 2005a, P-waves from cross-correlation of seismic noise: Geophysical Research Letters, **32**, L19303, doi: 10.1029/2005GL023803.

Roux, P., K. G. Sabra, W. A. Kuperman, and A. Roux, 2005b, Ambient noise cross correlation in free space: Theoretical approach: The Journal of the Acoustical Society of America, **117**, 79–84, doi: 10.1121/1.1830673.

Sabra, K. G., P. Gerstoft, P. Roux, W. Kuperman, and M. C. Fehler, 2005a, Extracting time-domain Green's function estimates from ambient seismic noise: Geophysical Research Letters, **32**, L03310, doi: 10.1029/2005GL023155.

Sabra, K. G., P. Gerstoft, P. Roux, W. Kuperman, and M. C. Fehler, 2005b, Surface wave tomography from microseisms in Southern California: Geophysical Research Letters, **32**, L14311, doi: 10.1029/2005GL023155.

Schimmel, M., E. Stutzmann, and J. Gallart, 2011, Using instantaneous phase coherence for signal extraction from ambient noise data at a local to a global scale: Geophysical Journal International, **184**, 494–506, doi: 10.1111/j.1365-246X.2010.04861.x.

Seydoux, L., J. de Rosny, and N. M. Shapiro, 2017, Pre-processing ambient noise cross-correlations with equalizing the covariance matrix eigenspectrum: Geophysical Journal International, **210**, 1432–1449, doi: 10.1093/gji/ggx250.

Seydoux, L., N. Shapiro, J. Rosny, and M. Landès, 2016, Spatial coherence of the seismic wavefield continuously recorded by the USArray: Geophysical Research Letters, **43**, 9644–9652, doi: 10.1002/2016GL070320.

Shapiro, N. M., and M. Campillo, 2004, Emergence of broadband Rayleigh waves from correlations of the ambient seismic noise: Geophysical Research Letters, **31**, L07614, doi: 10.1029/2004GL019491.

Shapiro, N. M., M. Campillo, L. Stehly, and M. H. Ritzwoller, 2005, High-resolution surface-wave tomography from ambient seismic noise: Science, **307**, 1615–1618, doi: 10.1126/science.1108339.

Shapiro, N. M., M. Ritzwoller, and G. Bensen, 2006, Source location of the 26 sec microseism from cross-correlations of ambient seismic noise: Geophysical Research Letters, **33**, L18310, doi: 10.1029/2006GL027010.

Snieder, R., 2004, Extracting the Green's function from the correlation of coda waves: A derivation based on stationary phase: Physical Review E, **69**, 046610, doi: 10.1103/PhysRevE.69.046610.

Tsai, V. C., 2009, On establishing the accuracy of noise tomography travel-time measurements in a realistic medium: Geophysical Journal International, **178**, 1555–1564, doi: 10.1111/j.1365-246X.2009.04239.x.

Tsai, V. C., 2011, Understanding the amplitudes of noise correlation measurements: Journal of Geophysical Research: Solid Earth, **116**, B09311, doi: 10.1029/2011JB008483.

Wapenaar, K., 2004, Retrieving the elastodynamic Green's function of an arbitrary inhomogeneous medium by cross correlation: Physical Review Letters, **93**, 254301, doi: 10.1103/PhysRevLett.93.254301.

Wapenaar, K., and J. Fokkema, 2006, Green's function representations for seismic interferometry: Geophysics, **71**, no. 4, SI33–SI46, doi: 10.1190/1.2213955.

Weaver, R. L., 2010, Equipartition and retrieval of Green's function: Earthquake Science, **23**, 397–402, doi: 10.1007/s11589-010-0738-2.

Weaver, R. L., and O. I. Lobkis, 2001a, On the emergence of the Green's function in the correlations of a diffuse field: The Journal of the Acoustical Society of America, **110**, 894–903, doi: 10.1121/1.1385566.

Weaver, R. L., and O. I. Lobkis, 2001b, Ultrasonics without a source: Thermal fluctuation correlations at MHz frequencies: Physical Review Letters, **87**, 134301, doi: 10.1103/PhysRevLett.87.134301.

Weaver, R. L., and O. I. Lobkis, 2006, Diffuse fields in ultrasonics and seismology: Geophysics, **71**, no. 4, SI5–SI9, doi: 10.1190/1.2212247.

Wu, C., A. Delorey, F. Brenguier, C. Hadziioannou, E. G. Daub, and P. Johnson, 2016, Constraining depth range of S wave velocity decrease after large earthquakes near Parkfield, California: Geophysical Research Letters, **43**, 6129–6136, doi: 10.1002/2016GL069145.

Zhang, J., and P. Gerstoft, 2014, Local-scale cross-correlation of seismic noise from the Calico fault experiment: Earthquake Science, **27**, 311–318, doi: 10.1007/s11589-014-0074-z.